Antireflective Transparent Oleophobic Surface by Non-Interacting Cavities

Juan Rombaut[1], Rinu Abraham Maniyara[1], Robert A. Bellman[2], Daniel F. Acquard[2], Adra S. Baca[2], Johann Osmond[1], Wageesha Senaratne[2], Mark Alejandro Quesada[2], David Baker[2], Prantik Mazumder[2], Valerio Pruneri*[1,3]*

[1] ICFO- Institut de Ciències Fotòniques, The Barcelona Institute of Science and Technology, 08860 Castelldefels (Barcelona), Spain.

[2] Corning Research and Development Corporation, Sullivan Park, Corning, New York 14831, United States.

[3] ICREA- Institució Catalana de Recerca i Estudis Avançats, 08010, Barcelona, Spain.

KEYWORDS Antireflective, Oleophobic, Transparent surface, nanostructured optical surfaces, Micro-Nano manufacturing, self-cleaning, surface wetting, cavities

ABSTRACT

Oleophobic surfaces have been so far realized using complex micro-scale and nano-scale re-entrant geometries where primary and secondary structures or overhang geometries are typically required. Here we propose a new design to create them with non-interacting cavities. The suspension of liquid droplets relies on the mechanism of compression of air under the meniscus

leading to stable composite oil-air-solid interfaces. To demonstrate the concept, we make oleophobic surfaces, with contact angle for oleic acid of about 130º (and Hexadecane about 110º), using both micro-holes in silicon and nano-holes in glass. Thanks to the subwavelength dimensions and antireflection effect of the nano-holes, the glass substrate also shows a high degree of optical transparency with optical transmission exceeding that of the initial bare substrate. Crockmeter tests without any significant change of morphology, optical and wetting properties after more than 500 passes also confirm the high mechanical durability of the nano-hole surface. The results indicate the possibility of using the proposed oleophobic surfaces for a wide range of applications, including self-cleaning transparent windows, windshields for automobiles and aircrafts.

Introduction

The contact angle of a liquid on a substrate is a function of the surface energy and surface roughness of the substrate [1]. For a perfectly flat surface, it is only dependent on the surface energy and is given by the Young contact angle, θ_Y [2]. The maximum Young contact angles obtained on low surface energy flat surfaces, such as fluoropolymer coated surfaces, are ~110-120 degrees for water and ~70-80 degrees for oil [3]. Surface roughness is required to attain super-hydrophobicity, oleophobicity and/or super-oleophobicty. One of the most cited naturally occurring super-hydrophobic surfaces is the Lotus leaf on which water contact angle greater than 150º has been observed [4–7]. This super-hydrophobicity has been ascribed to both surface chemistry as well as surface roughness. Based on the fundamental understanding gleaned from such studies, many artificial super-hydrophobic and super-oleophobic substrates consisting of surface asperities, composed of regularly arranged vertical pillars of square, circular or other geometric cross-section [8–11], and triangular spikes [12], have been fabricated with numerous practical and industrial applications [13–19]. It has been experimentally observed and theoretically predicted that a liquid

droplet placed on such asperities could assume one of the two configurations; the Wenzel (W) state [20] or the Cassie-Baxter (CB) state [21]. In the W state, the liquid fully invades the space between the asperities and wets the entire solid surface underneath itself. The contact angle in this state is given by the W model:

$$\cos\theta_w = r_w \cos\theta_Y \qquad (1)$$

where r_W is the roughness parameter defined as the ratio of the actual liquid-solid interfacial area to the projected planar area and is always greater than one [22]. In the CB configuration the droplet resides on the top of the asperities without invading the space in-between. Much of the liquid surface is suspended in air and a composite interface is made with solid-liquid and air-liquid interfaces. The contact angle in this configuration is given by the CB model:

$$\cos\theta_{CB} = -1 + f(1 + r_f \cos\theta_Y) \qquad (2)$$

where, f is the area fraction of solid-liquid interface and r_f is the roughness factor of the wetted area [22]. Between these two equilibrium configurations, the one with lower free energy is thermodynamically more stable [23,24]. It has been theoretically and experimentally demonstrated that for any liquid which has Young contact angle less than 90 degrees, such as oil, the W state is always energetically favorable. An oil droplet positioned over such asperities would be unstable and undergo a transition from the CB to W state [22–26]. This is the reason behind the difficulty of attaining an oleophobic condition on a simple rough surface. The only few cases when oleophobic and super-oleophobic surfaces have been fabricated correspond to complex surfaces consisting of re-entrant and overhang or undercut structures [25–35]. The purpose of the re-entrant or overhang geometry is to create an energy barrier to the wetting transition from CB to W state. It has been claimed that the only possible way of creating a robust oleophobic state is through the fabrication of re-entrant geometry [25,26]. However, such complex surfaces are difficult and expensive to

fabricate and may not be suitable for industrial applications. Therefore, there is great value in developing geometries that are easy to fabricate, yet providing oleophobic and super-oleophobic characteristics.

Results and discussion

In this paper, we propose a new design where oleophobic surfaces can be made using simple geometries that do not require re-entrant structures. This can be achieved through the creation of *non-interacting cavities* on the substrate surface. An example of such non-interacting cavities is shown in Figure 1a. Square cavities of side 'a', spacing 'b' and depth 'H' are fabricated either in silicon substrate via standard photo-lithography and reactive ion etching. The argument behind the non-interacting cavities is to physically trap air inside when a liquid meniscus is formed at the top of the cavities. This is a distinctive feature compared to the asperities where the air can leave the space under the advancing oil meniscus through interconnecting pathways. As the meniscus invades the cavity, the air gets compressed which raises its pressure. The increased pressure of the trapped air opposes the advancing meniscus and a mechanical equilibrium could be reached between the downward capillary force and the upward pressure force exerted by the compressed air as shown in Figure 1b. We differentiate this state from the CB and W states as Partially Wetting (PW) state. A simplified mechanistic model of the PW state can be developed as follows. If the equilibrium penetration depth is h^*, assuming ideal gas law and adiabatic compression, the pressure of entrapped air is given by:

$$P_{air}(h^*) = P_\infty \left[\frac{a^2 H}{V_{air}(h^*)}\right]^\gamma \qquad (3)$$

Where P_∞ is atmospheric pressure, $P_{air}(h^*)$ and $V_{air}(h^*)$ are the pressure and the volume of the compressed air inside the cavity at the equilibrium condition and γ is the adiabatic index. The volume of air is given by:

$$V_{air}(h^*) = a^2(H - h^*) + \frac{a^3}{6\sqrt{\pi}}\left[3\frac{1-\sin\theta_Y}{\cos\theta_Y} + \left(\frac{1-\sin\theta_Y}{\cos\theta_Y}\right)^3\right] \quad (4)$$

where the second term is the cap volume under the hemispherical cap [36]. The condition for mechanical equilibrium is:

$$P_{air}(h^*) - P_\infty = \frac{4\sigma\cos\theta_Y}{a} \quad (5)$$

The solution of equilibrium penetration depth can be found from equations 3-5 as:

$$\frac{h^*}{H} = 1 - \left[\frac{aP_\infty}{aP_\infty + 4\sigma\cos\theta_Y}\right]^{1/\gamma} + \frac{\pi a}{6H}\left[3\frac{1-\sin\theta_Y}{\cos\theta_Y} + \left(\frac{1-\sin\theta_Y}{\cos\theta_Y}\right)^3\right] \quad (6)$$

Using the equilibrium depth, h^* of equation (6), the overall contact angle of the partially wetted state could be calculated as:

$$\cos\theta_{PW} = -1 + f(1 + r_f\cos\theta_Y) \quad (7)$$

with

$$f = 1 - \frac{1}{(1+b/a)^2} \quad (8a)$$

$$r_f = 1 + \frac{4ah^*}{f(a+b)^2} \quad (8b)$$

Calculation of the contact angle corresponding to various cavity designs is presented in Table 1 for two low surface tension liquids – hexadecane and oleic acid. The Young contact angles, θ_Y are equal to 70° and 80° for hexadecane and oleic acid and the surface tension values are 32.5

dynes/cm and 27.5 dynes/cm, respectively. The CB calculation corresponds to the case where the liquid drops remain on the very top of the cavities. This state offers the highest contact angle. The W calculation corresponds to the case when the liquids fully invades and fill up the cavities. This state leads to the lowest contact angle. The PW calculation corresponds to the model developed above where the liquid meniscus partially invades the cavities and is equilibrated by the pressure of the compressed air. The contact angle values of the PW state is very close to the CB contact angles. Liquid contact angles were measured on the fabricated cavities of Figure 1a after coating with a fluoropolymer corresponding to the same dimensions as the calculations. The measured contact angle values are compared with the three theoretical models in Table 1. They fall in between PW and W models and closer to the PW model than the oleophilic W model. This confirms that oleophobic state has been achieved on the substrate through the non-interacting cavities.

The PW state micro-holes in silicon described above are not suitable for applications, which need optical transparency, e.g. protecting windows, touch screens, car windshields and solar panels. For such applications, an optically transparent substrate material must be used, that means that the PW state structures must be smaller than the light wavelength. Their dimensions should not exceed about 150 nm for the visible range, so that scattering effects are avoided. In order to demonstrate this, we used a substrate of glass, fused silica composition, and created nano-holes in it by scalable self-assembly lithography (see fig. 2 and methods section for a detailed description). The resulting subwavelength structures show an increased optical transmission with respect to bare (not surface structured) substrate thanks to the antireflection effect while still keeping oleophobic properties due to air trapping. From fig. 3a one can see that the reflection of the structured nanohole front surface is almost suppressed, considering that the residual reflection (about 3%) is basically

entirely due to the flat back suface. The reflection of a fused silica bare substrate with both surface contributions is about 6.5%. Correspondingly, the optical transmission reaches values in excess of 95%. The nanohole structures are oleophillic right after the making process and cleaning in SC1 (mixture of deionized water, NH_4OH and H_2O_2 (5:1:1) used at 75-80°C for 10 minutes) and become oleophobic (contact angle for oil of about 120º) after the application of a fluorosilane (fig. 3b). Note that without structuring the contact angle of a glass surface coated with fluosilane would be much lower, about 75º, making evident the effect of the air trapping nano-hole cavities to provide oleophobicity.

Focusing on the potential applications where the proposed structures can be applied, the crockmeter test is a valuable tool to measure the mechanical resistance of the fabricated samples. It can emulate the action of a human finger, which makes it relevant for display screen applications by signaling any wear or damage. The standard crock-meter test, that provides reproducible and comparable results, uses a constant force (9N) over a 2 cm^2 area applied through a standard rubbing material (microfiber cloth). It is significant to see the response of the nano-structured glass surfaces, especially the nano-holes resistance, after a high number of crock-meter passes. Before and after the test, the samples were characterized by scanning electron microscopy (SEM) (fig 4.a) and measuring the wetting properties (fig 4.b). The results prove that the nanocavities can withstand more than 500 passes as there is no sign of any significant change in the SEM or wetting response. This is crucial for many applications where the transparent omniphobic surfaces are touched, either because of functional reasons (e.g. touch display screens) or cleaning purposes (e.g. glass windows).

Methods

Fabrication of micro-holes on silicon wafer.

The fabrication process to create the silicon micro-holes was the following. Silicon wafer surface was firstly cleaned in acetone followed by ethanol in ultrasonic bath, each process lasting 10 min. The substrates were then rinsed in deionized water and dried with nitrogen gas. On dehydrated silicon substrate, photoresist AZ5214 (from Microchemicals) was spin coated and soft baked at 100 ºC. The holes structures were then patterned by laser lithography at 405 nm wavelength (Microtech Laserwriter LW405B). After development, the cavities were etched by a reactive ion etching (RIE) system (Plasmalab System 100, Oxford Instruments) using C_4F_8 and SF_6 chemistry. After etching, remaining photoresist was removed by acetone.

Fabrication of nano-hole subwavelength structure on glass surface.

The fabrication process to create the nano-hole subwavelength structure on the glass surface is shown in figure 2. Double-side, optically polished, ultraviolet-fused silica glass substrates, with a thickness of 1mm and an area of 1 inch square, were used. The surfaces were cleaned in acetone followed by ethanol in ultrasonic bath for 10 min each. The substrates were then rinsed in deionized water and dried with nitrogen gas. A uniform monolayer of polystyrene (PS) nanobeads of diameter 500nm (from Sigma Aldrich) was deposited on the glass substrate by using the Langmuir Blodgett method (KSV NIMA LB from Biolin Scientific) - fig2. (a). The size of the chosen nanobeads comes from the previous optimization of the process. The diameter of the nanobeads is a key factor that determines the period between the holes. With larger beads, the period is increased. The deposited PS nanobeads were then shrunk with oxygen plasma by using a RIE system (Plasmalab System 100, Oxford Instruments) - fig2. (b). With this step, the size of the beads is reduced while the position is maintained. Changing the etching time, the top diameter

of the final nano-holes is directly modified. The first two steps are key points to customize the final structure. A thin layer of copper 50 nm was then deposited with a magnetron sputtering system (ATC Orion 8, AJA International, INC) - fig2. (c). The nano-beads were subsequently removed from the structure using Kapton tape, leaving a copper mask with an array of nano-holes - fig2. (d). The copper mask was used during a RIE process to etch the surface of the glass. Different etching times allowed making nano-hole structures of different depths. After RIE, the samples were immersed in ammonium persulfate for 10 minutes to remove the residual metal mask - fig2. (e). Finally, the surface of the structure was activated using oxygen plasma (PVA TePla 300 Semi-Auto Plasma Asher), dip coated with a low surface energy fluorosilane for 3 minutes and dried at 50ºC for one hour in a regular oven leading to an oleophobic surface.

Special optimization can be performed modifying the size and period of the PS nanobeads and the depth of the nano-holes. By adjusting these parameters, it is possible to obtain different optical and wetting properties depending on the application.

Optical, wetting and mechanical characterization.

The total transmittance and reflectance were measured using a UV-vis-NIR spectrophotometer (PerkingElmer Lambda 950) in the wavelength range of 380-1500nm. Haze measurements were performed using Haze-meter (BYK-Gardner 4601 haze-gloss). The nano-holes were examined with a field-emission scanning electron microscope (FEG-SEM, Inspect F, FEI Systems). Oleic acid and hexadecane contact angles were measured and averaged at multiple positions on the surface of samples by using a drop shape analysis system (DSA-100, Krüss GmbH).

The mechanical resistance tests were performed by a homologate electronic crockmeter (M238BB, SDLATLAS). Standard weight of 9N was used with a stroke length of 50mm and the abrandant surface was a crockmeter microfiber cloth.

Alternate method to produce nano-hole surface strctures.

An alternate method to produce the nano-hole (waffle) pattern is presented in the supporting information. Here, in brief, after the shrinkage of the PS beads, a transparent SiO film is deposited. Once the PS beads are removed, transparent nano-hole structures are formed which show both antireflection and oleophobic properties, similar to the aforementioned structures directly engraved in the glass surface.

Conclusions

We have proposed and demonstrated a new antireflective, transparent and oleophobic surface based on non-interacting cavities without the need of re-entrant or overhang structures. The approach is applicable to transparent substrates, such as glass, provided that subwavelength, nanometric scale, holes (cavities) are created. The antireflective effect comes from a smooth refractive index gradient at the interface associated to the conical shape of the nanoholes. When the nanostructure has a subwavelength dimension, light scattering becomes negligible, thus preserving the directionality of the transmitted beams. The phobic behavior is attributed to the pressure generated by the air trapped in the holes (cavities) underneath the liquid. We name the effect partial wetting state. As shown in the paper, the partial wetting nano-holes can be made by using scalable techniques for large areas that can have an impact in antismudge touch screens, automobile windshields, solar panels and other applications that needs high transmission and self-cleaning properties.

FIGURES

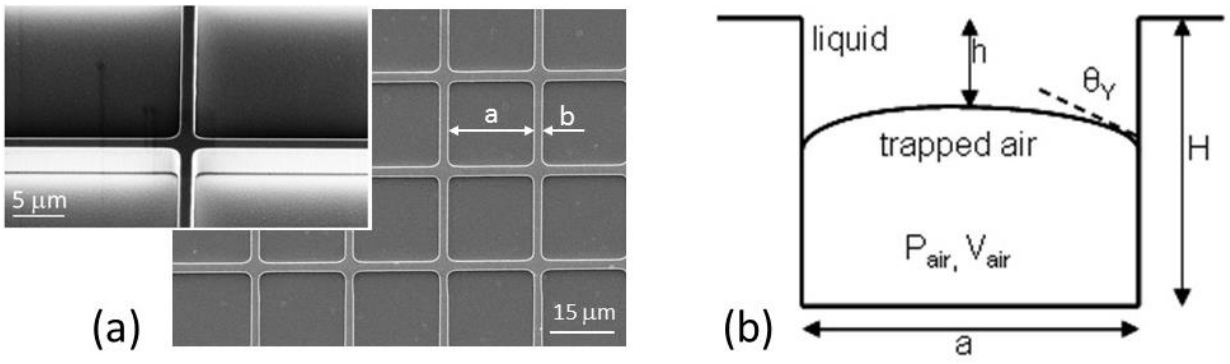

Figure 1. (a) SEM pictures of square non-interacting cavity structures fabricated on the surface of a silicon substrate (b) Schematic of the mechanism of oleophobicity in non-interacting cavities

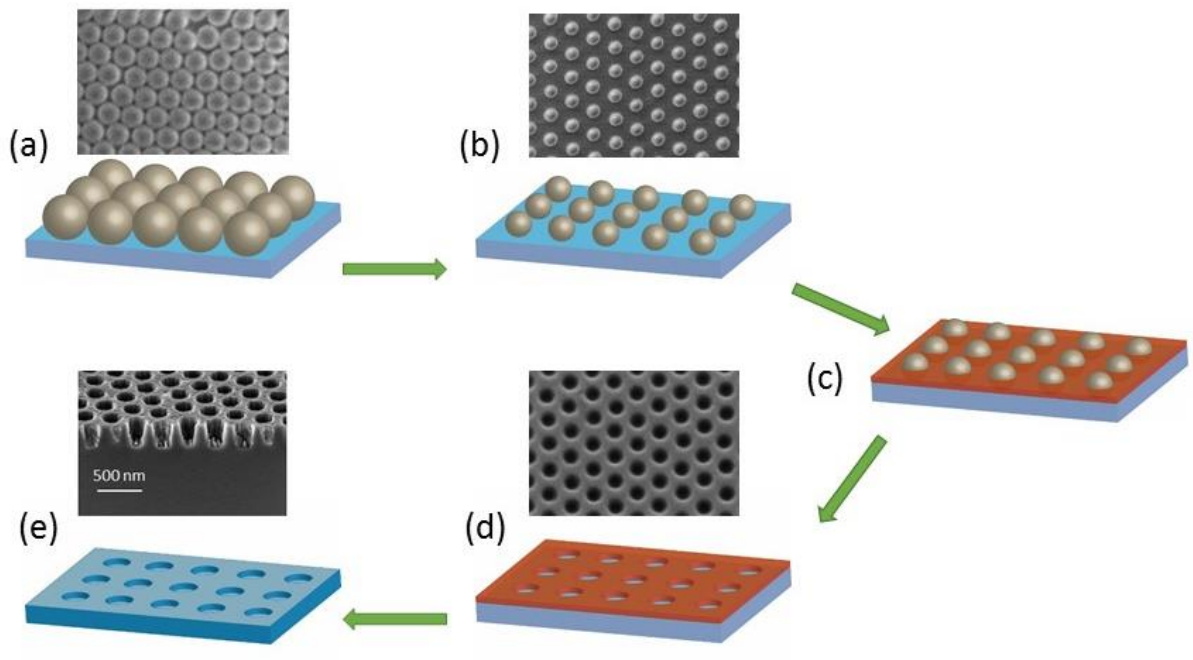

Figure 2. Process flow to realize subwalength oleophobic nano-hole structures which are also transparent in the visible and near infrared range: deposition of polystyrene nano-beads (a); shrinking using oxygen plasma (b); deposition of copper film (c); reactive ion etching (d) and removal of copper mask (e). The SEM pictures taken at different steps are on the same scale. For a detailed description of the fabrication steps please refer to method section.

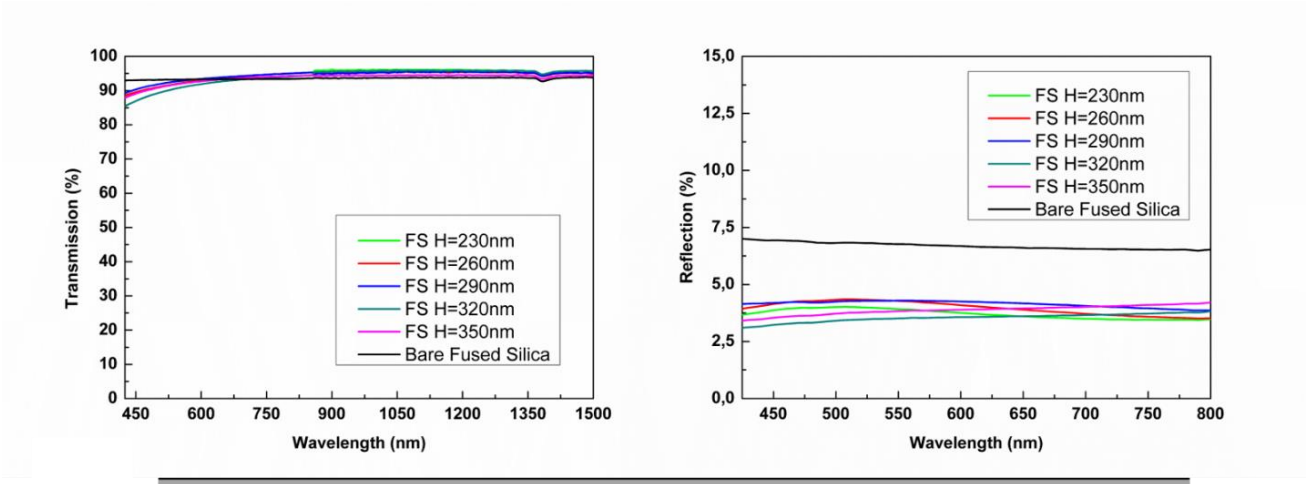

(a)

Sample	H (nm)	a (nm)	b (nm)
FS H=230nm	230	235±6	40±6
FS H=260nm	260	230±5	48±5
FS H=290nm	290	232±8	68±9
FS H=320nm	320	235±9	46±6
FS H=350nm	350	225±7	45±4

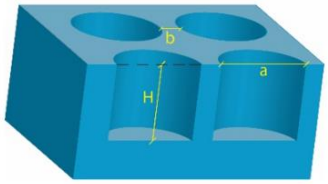

(b.1)

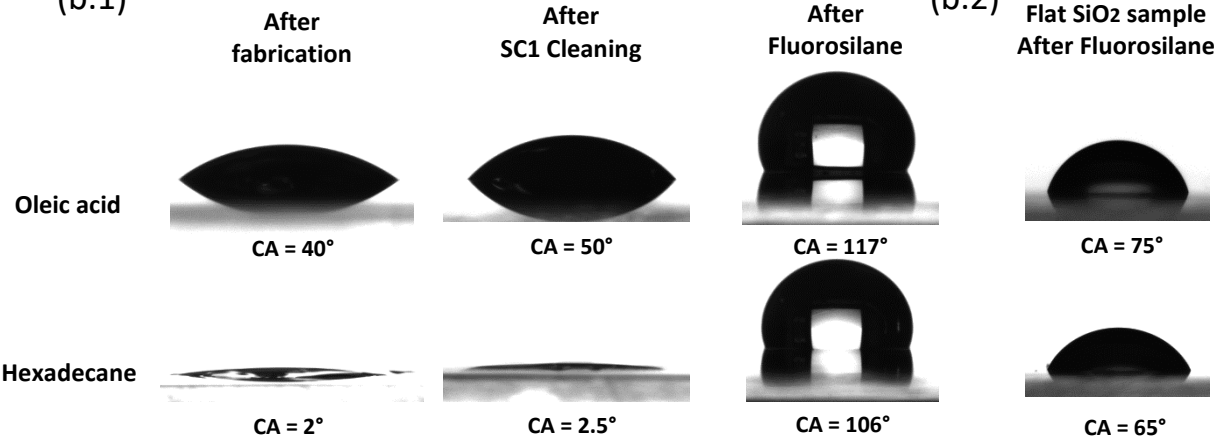

(b.2)

Figure 3. Optical and wetting properties of subwavelength nanohole structures: optical transmission and reflection together with sample description (a); Contact angle (CA) for oleic acid and hexadecane for nanostructured sample H=230nm (b.1) and comparison with flat SiO2 sample after fluorosilane (b.2).

(a)

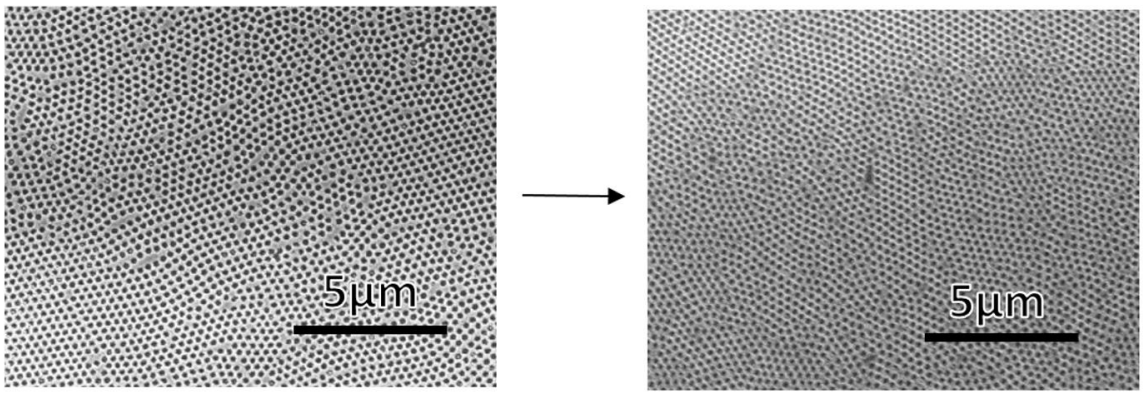

(b)

Before crockmeter test		After crockmeter test	
Oleic acid	*Hexadecane*	*Oleic acid*	*Hexadecane*
120 ± 3	105 ± 2	118 ± 4	105 ± 3

Figure 4. Mechanical resistance test results after 500 passes of crockmeter with 9N force over 2cm^2 contact area. SEM Images of the nano-holes before and after the crockmeter test (a) and wetting properties (oleic acid and hexadecane contact angles in degree) before and after the crockmeter test (b).

TABLES

Sample ID	Dimensions	Experiment: Fluorosilane		Calculated: Fluorosilane, PW		Calculated: Fluorosilane, CB		Calculated: Fluorosilane, W	
		Oleic acid	*Hexadecane*	*Oleic acid*	*Hexadecane*	*Oleic acid*	*Hexadecane*	*Oleic acid*	*Hexadecane*
A	*a = 18.6 , b = 1.4 H = 1.07*	127 ± 5	115 ± 3	145.7	139.28	147.3	144.95	78.0	65.79
B	*a = 20.5 , b = 1.5 H = 2.4*	128 ± 2	109 ± 2	146.1	139.56	147.7	145.41	75.9	61.24
C	*a = 20 , b = 4 H = 2*	126 ± 2	111 ± 3	129	122.71	129.9	126.15	77.2	64.09
D	*a = 20 , b = 2 H = 2*	125 ± 1	106 ± 2	141.4	135.09	142.8	140.09	76.6	62.93

Table 1. Compilation of calculated and measured oleic acid and hexadecane contact angle data (in degree) of microstructure silicon samples after coating with fluorosilane. The dimensions of a, b and H are in μm. PW=partial wetting, CB=Cassie-Baxter and W=Wenzel

ASSOCIATED CONTENT

The supporting Information is available free of charge.

An alternate method to produce the nano-hole (waffle) pattern. (file type, PDF)

AUTHOR INFORMATION

Corresponding Author

*(V.P) E-mail: valerio.pruneri@icfo.es

*(P.M) E-mail: mazumderp@corning.com.

Author Contributions

The manuscript was written through contributions of all authors. All authors have given approval to the final version of the manuscript.

Notes

The authors declare no competing financial interest.

ACKNOWLEDGMENT

We acknowledge financial support from the Spanish Ministry of Economy and Competitiveness through the "Severo Ochoa" Programme for Centres of Excellence in R&D (SEV-2015-0522) and OPTO-SCREEN (TEC2016-75080-R), from Fundació Privada Cellex, and from Generalitat de Catalunya trough the CERCA program. Partial support was also provided by Corning.

REFERENCES

(1) Lundgren, M.; Allan, N. L.; Cosgrove, T. Modeling of Wetting: A Study of Nanowetting at Rough and Heterogeneous Surfaces. *Langmuir* **2007**, *23* (3), 1187–1194.

(2) Young, T. On the Cohesion of Fluids. *Trans R.Soc.* **1805**, *95*, 65–89.

(3) Mazumder, P.; Jiang, Y.; Baker, D.; Carrilero, A.; Tulli, D.; Infante, D.; Hunt, A. T.; Pruneri, V. Superomniphobic, Transparent, and Antire Fl Ection Surfaces Based on Hierarchical Nanostructures. *Nano Lett.* **2014**, 4677–4681.

(4) Barthlott, W.; Neinhuis, C. Purity of the Sacred Lotus, or Escape from Contamination in Biological Surfaces. *Planta* **1997**, *202* (1), 1–8.

(5) Ensikat, H. J.; Ditsche-Kuru, P.; Neinhuis, C.; Barthlott, W. Superhydrophobicity in Perfection: The Outstanding Properties of the Lotus Leaf. *Beilstein J. Nanotechnol.* **2011**, *2* (1), 152–161.

(6) Gao, L.; McCarthy, T. J. The “lotus Effect” explained: Two Reasons Why Two Length Scales of Topography Are Important. *Langmuir* **2006**, *22* (7), 2966–2967.

(7) Yamamoto, M.; Nishikawa, N.; Mayama, H.; Nonomura, Y.; Yokojima, S.; Nakamura, S.; Uchida, K. Theoretical Explanation of the Lotus E Ff Ect: Superhydrophobic Property Changes by Removal of Nanostructures from the Surface of a Lotus Leaf. *Langmuir* **2015**.

(8) He, B.; Patankar, N. A.; Lee, J. Multiple Equilibrium Droplet Shapes and Design Criterion for Rough Hydrophobic Surfaces. *Langmuir* **2003**, *19* (12), 4999–5003.

(9) Nosonovsky, M.; Bhushan, B. Patterned Nonadhesive Surfaces: Superhydrophobicity and

Wetting Regime Transitions. *Langmuir* **2008**, *24* (4), 1525–1533.

(10) Öner, D.; McCarthy, T. J. Ultrahydrophobic Surfaces. Effects of Topography Length Scales on Wettability. *Langmuir* **2000**, *16* (20), 7777–7782.

(11) Lu, Y. Surface & Coatings Technology Fabrication of a Lotus Leaf-like Hierarchical Structure to Induce an Air Lubricant for Drag Reduction Electroless Copper Electrodeposition Cu-Ni Modification Lotus Leaf-like Surface. *Surf. Coat. Technol.* **2017**, *331* (October), 48–56.

(12) Lafuma, A.; Quéré, D. Superhydrophobic States. *Nat. Mater.* **2003**, *2* (7), 457–460.

(13) Paven, M.; Mammen, L.; Vollmer, D. *Superamphiphobic Coatings in Real Applications*; The Royal Society of Chemistry, 2016.

(14) Milionis, A.; Bayer, I. S.; Loth, E. Recent Advances in Oil-Repellent Surfaces. *Int. Mater. Rev.* **2016**, *61* (2), 101–126.

(15) Jiang, T.; Guo, Z.; Liu, W. Biomimetic Superoleophobic Surfaces: Focusing on Their Fabrication and Applications. *J. Mater. Chem. A* **2015**, *3* (5), 1811–1827.

(16) Bellanger, H.; Darmanin, T.; Ta, E. Chemical and Physical Pathways for the Preparation of Superoleophobic Surfaces and Related Wetting Theories. *Chem. Rev.* **2014**.

(17) Liu, K.; Tian, Y.; Jiang, L. Progress in Materials Science Bio-Inspired Superoleophobic and Smart Materials : Design , Fabrication , and Application. *Prog. Mater. Sci.* **2013**, *58* (4), 503–564.

(18) Kota, A. K.; Kwon, G.; Tuteja, A. The Design and Applications of Superomniphobic

Surfaces. *NPG Asia Mater.* **2014**, *6* (7), e109-16.

(19) Pan, Z.; Cheng, F.; Zhao, B. Bio-Inspired Polymeric Structures with Special Wettability and Their Applications : An Overview. *Polymers (Basel).* **2017**, 32–39.

(20) Wenzel, R. N. Surface Roughness and Contact Angle. *Ind. Eng. Chem.* **1936**, No. 28, 988–994.

(21) Cassie, A. B. D.; Baxter, S. Wettability of Porous Surface. *Trans. Faraday Soc.* **1944**, *40*, 546–551.

(22) Marmur, A. Wetting on Hydrophobic Rough Surfaces: To Be Heterogeneous or Not to Be? *Langmuir* **2003**, *19* (20), 8343–8348.

(23) Patankar, N. a. On the Modeling of Hydrophobic Contact Angles on Rough Surfaces On the Modeling of Hydrophobic Contact Angles on Rough. *Society* **2003**, *19* (January), 1249–1253.

(24) Patankar, N. A. Transition between Superhydrophobic States on Rough Surfaces. *Langmuir* **2004**, *20* (17), 7097–7102.

(25) Tuteja, A.; Choi, W.; Ma, M.; Mabry, J. M.; Mazzella, S. A.; Rutledge, G. C.; Mckinley, G. H.; Cohen, R. E. Designing Superoleophobic Surfaces. *Sci. Reportsience* **2007**, No. December, 1618–1623.

(26) Tuteja, A.; Choi, W.; Mabry, J. M.; McKinley, G. H.; Cohen, R. E. Robust Omniphobic Surfaces. *Proc. Natl. Acad. Sci.* **2008**, *105* (47), 18200–18205.

(27) Cao, L.; Hu, H. A.; Gao, D. Design and Fabrication of Micro-Textures for Inducing a

Superhydrophobic Behavior on Hydrophilic Materials. *Langmuir* **2007**, *23* (8), 4310–4314.

(28) Hsieh, C.T.; Chen, J.M; Kuo, R.R.; Lin, T.S.; Wu, C. F. Influence of Surface Roughness on Water - and Oil - Repellent Surfaces Coated with Nanoparticles. *Appl. Surf. Sci.* **2005**, *240*, 318–326.

(29) Choi, H. J.; Choo, S.; Shin, J. H.; Kim, K. I.; Lee, H. Fabrication of Superhydrophobic and Oleophobic Surfaces with Overhang Structure by Reverse Nanoimprint Lithography. *J. Phys. Chem. C* **2013**, *117* (46), 24354–24359.

(30) Lee, S. E.; Kim, H. J.; Lee, S. H.; Choi, D. G. Superamphiphobic Surface by Nanotransfer Molding and Isotropic Etching. *Langmuir* **2013**, *29* (25), 8070–8075.

(31) Brown, P. S.; Bhushan, B. Durable, Superoleophobic Polymer-Nanoparticle Composite Surfaces with Re-Entrant Geometry via Solvent-Induced Phase Transformation. *Sci. Rep.* **2016**, *6* (February), 1–11.

(32) Kim, J.; Lin, P.; Kim, W. S. Mechanically Robust Super-Oleophobic Stamp for Direct Stamping of Silver Nanoparticle Ink. *Thin Solid Films* **2012**, *520* (13), 4339–4343.

(33) Dufour, R.; Perry, G.; Harnois, M.; Coffinier, Y.; Thomy, V.; Senez, V.; Boukherroub, R. From Micro to Nano Reentrant Structures: Hysteresis on Superomniphobic Surfaces. *Colloid Polym. Sci.* **2013**, *291* (2), 409–415.

(34) Kang, S. M.; Kim, S. M.; Kim, H. N.; Kwak, M. K.; Tahk, D. H.; Suh, K. Y. Robust Superomniphobic Surfaces with Mushroom-like Micropillar Arrays. *Soft Matter* **2012**, *8* (33), 8563.

(35) Chen, L.; Guo, Z. Outmatching Superhydrophobicity: Bio-Inspired Re-Entrant Curvature

for Mighty Superamphiphobicity in Air. *J. Mater. Chem. A* **2017**, No. February 2010, 14480–14507.

(36) Pesse, A. V.; Warrier, G. R.; Dhir, V. K. An Experimental Study of the Gas Entrapment Process in Closed-End Microchannels. *Int. J. Heat Mass Transf.* **2005**, *48* (25–26), 5150–5165.

TABLE OF CONTENTS